HOKKAIDO UNIVERSITY

Title	Electrocatalytic nitrate and nitrous oxide reduction at interfaces between Pt-Pd nanoparticles and fluorine-doped tin oxide
Author(s)	Sarker, Abinash Chandro; Kato, Masaru; Yagi, Ichizo
Citation	Electrochimica Acta, 425, 140628 https://doi.org/10.1016/j.electacta.2022.140628
Issue Date	2022-09-01
Doc URL	https://hdl.handle.net/2115/93023
Rights	© 2022. This manuscript version is made available under the CC-BY-NC-ND 4.0 license http://creativecommons.org/licenses/by-nc-nd/4.0/
Rights(URL)	https://creativecommons.org/licenses/by-nc-nd/4.0/
Type	journal article
File Information	APD_Manuscript_Final_Version.pdf



Hokkaido University Collection of Scholarly and Academic Papers : HUSCAP

Electrocatalytic nitrate and nitrous oxide reduction at interfaces between Pt-Pd nanoparticles and fluorine-doped tin oxide

Abinash Chandro Sarker,[a] Masaru Kato,[a,b]* and Ichizo Yagi[a,b]*

[a] Graduate School of Environmental Science, Hokkaido University, N10W5, Kita-ku, Sapporo 060-0810, Japan

[b] Faculty of Environmental Earth Science, Hokkaido University, N10W5, Kita-ku, Sapporo 060-0810, Japan

*Corresponding authors: masaru.kato@ees.hokudai.ac.jp (MK), iyagi@ees.hokudai.ac.jp (IY)

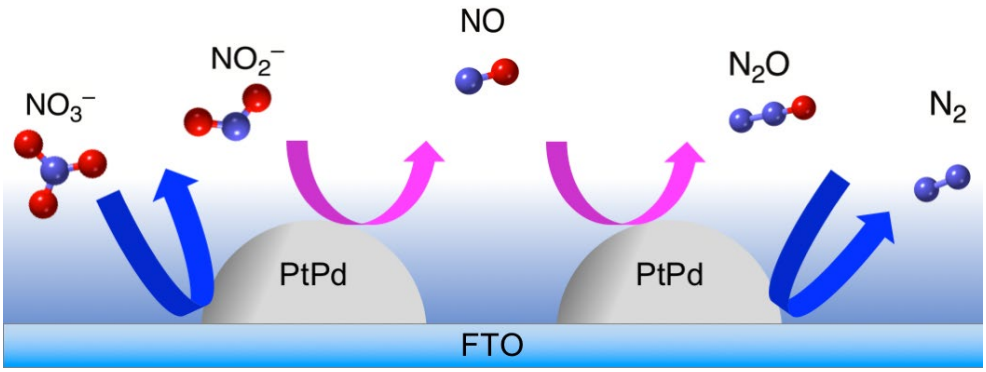
Abstract

We report the preparation of Pt and/or Pd nanoparticle-deposited fluorine-doped tin oxide (FTO) electrodes by an arc-plasma deposition (APD) technique and their electrocatalytic activity for nitrate (NO_3^-), nitrite (NO_2^-), nitric oxide (NO), and nitrous oxide (N_2O) reduction reactions in acidic media. Cyclic voltammetry of the electrodes revealed that the co-presence of Pt and Pd on FTO showed higher catalytic activity than Pt or Pd on FTO for the NO_3^- reduction reaction, where the PtPd/Sn interface acts as the catalytic active site. The PtPd/Sn interface also showed higher catalytic activity for the N_2O reduction reaction to dinitrogen than the Pt/Sn or Pd/Sn interfaces, whereas it showed no drastic contribution to the electrocatalytic NO_2^- and NO reduction reactions. Because the NO_3^- and N_2O reduction reaction occur in the potential region of hydrogen adsorption on Pt and Pd electrodes, the PtPd/Sn interface could enhance NO_3^- and N_2O adsorption and/or suppress the hydrogen adsorption. Our findings will be useful for the design of interfaces between noble metal mixture/alloy nanoparticles and Sn, leading to the practical application of denitrification to harmless dinitrogen.

Research highlights

- Pt, Pd and PtPd nanoparticles are deposited on FTO by arc-plasma deposition.
- The PtPd/Sn interface has higher NO_3RR activity than the Pt/Sn or Pd/Sn interface.
- The PtPd/Sn interface also has higher N_2ORR activity.
- The PtPd/Sn interface shows no drastic contribution to NO_2RR and NORR.

Graphical abstract



Keywords: Interface; Nanoparticle; Nitrate reduction reaction; Nitrous oxide reduction reaction; Platinum; Palladium; Arc plasma deposition.

1. Introduction

Contamination of nitrate anions (NO_3^-) in groundwater causes health threats: methemoglobinemia (blue baby syndrome) and human cancer, and environmental issues: global warming and depletion of the ozone layer [1–4]. Overuse of nitrogenous fertilizers in agricultural lands, animal feces, and industrial effluents are mainly accountable for NO_3^- contamination in groundwater [5]. Besides, nitrate-containing water runoff from urban surfaces and discharge of treated wastewater also lead to an increase in the amount of NO_3^- in groundwater [6]. NO_3^- concentration in drinking water exceeded 100 mg L^{-1} in some countries [7]. To minimize the health threats of NO_3^-, the World Health Organization (WHO) has recommended a maximum 50 mg L^{-1} as NO_3^- (~11 mg L^{-1} as NO_3^--N) in drinking water [8]. Therefore, an efficient technology for NO_3^- removal is required.

The electrocatalytic NO_3^- reduction reaction (NO_3RR) is the most promising technique because of no production of a secondary nitrate-containing waste stream, no requirement of additional chemicals, no possibility of bacterial contamination, and renewable energy friendliness [9–11]. NO_3^- can electrocatalytically be reduced to harmless dinitrogen (N_2) with the following by-products: nitrite (NO_2^-), nitric oxide (NO), nitrous oxide (N_2O), ammonium ion (NH_4^+), and hydroxylammonium ion (NH_3OH^+) [12–16]. Since N_2O is a greenhouse gas and a scavenger for the depletion of the ozone layer [4], efficient electrocatalysts for the NO_3RR with no production of N_2O are needed to keep the world sustainable.

Various electrocatalysts such as noble metals [9,14,17–19], binary metals [15,20–28], ternary metals [11,13,29,30], metal complexes [31–33], and metalloenzymes [34] have been already studied for the electrocatalytic NO_3RR. Generally, single metal electrodes including Pt and Pd are known to show poor electrocatalytic NO_3RR activity because of low NO_3^- adsorption energy as compared with hydrogen [14,35,36]. The modification of their surfaces with p-block metal adatoms significantly increases NO_3^- adsorption, leading to the acceleration of the rate-determining step of the NO_3^- reduction to NO_2^- [15,20–22,25,28,30,37]. For example, the surface modification of Pt and Pd electrodes with Sn enhances the NO_3RR activity, and the Sn/Pt and Sn/Pd interfaces act as the active sites, respectively. For the NO_2^- reduction reaction (NO_2RR), both Sn-

modified and unmodified Pt and Pd electrodes were found to be active [37]. For the NO reduction reaction (NORR) and N_2O reduction reaction (N_2ORR), the role of the Sn/Pt and Sn/Pd interfaces in the activity enhancement remains unclear. For ternary metallic electrodes, Sn-modified PdPt alloy (Sn/PdPt) electrodes have been studied only for the NO_3RR and show higher NO_3RR activity than the bimetallic counterparts of Sn-modified Pt or Pd electrodes and the suppression of N–H bond formation at the Sn/PdPt electrode increases the N_2 selectivity with decreasing the selectivity of NH_4^+ and NH_3OH^+ [13]. In a reverse system, Pt nanoparticle (NP)-modified fluorine-doped tin oxide (FTO) electrodes (Pt/FTO) were also found to be active for electrocatalytic NO_3RR, in which the Pt/Sn interface acts as the catalytic active site [28]. Since most of the studies for electrocatalytic NO_3RR have been done on Sn-modified noble metal electrodes, there is a lack of detailed investigations on reverse systems of Pt and/or Pd NPs on FTO for the electrocatalytic NO_3RR, NO_2RR, NORR, and N_2ORR, even though these systems have interfaces between Pt and/or Pd and Sn.

Herein, we report the electrocatalytic activity of Pt and/or Pd NP-deposited FTO electrodes for the NO_3RR in acidic media. The role of the PtPd/Sn interface was investigated in not only the NO_3RR but also the reduction of potential by-products: NO_2^-, NO, and N_2O. We have prepared three different electrodes of Pt and/or Pd NPs on FTO substrates: Pt/FTO, Pd/FTO, and Pt/Pd/FTO by an arc-plasma deposition (APD) method under high vacuum conditions. The APD method enables the direct deposition of metal NPs on the substrates by changing the number of pulses for controlling the amount of metal NPs. This method requires no multi-step preparation for the removal of surfactants or the impregnation processes, which are needed in solution-based methods [38]. Using the APD method, the deposited amounts of Pt and/or Pd NPs on FTO substrates were optimized for the NO_3RR to their pulse number, and then the NO_2RR, NORR, and N_2ORR activity of the optimized electrode was investigated to understand the role of the PtPd/Sn interface.

2. Experimental

2.1. Materials

Acetone, 2-propanol, 30% hydrogen peroxide, 28% ammonia, and 60% perchloric acid were purchased from Wako Pure Chemical Industries, Ltd. Sodium nitrate and

sodium nitrite were purchased from Kanto Chemical Co., Inc. Nitric oxide (NO) in Ar (50%) and nitrous oxide (N_2O, 99.5%) were purchased from Tomoe Shokai and GL Science, respectively. FTO glass sheets were purchased from SPD Laboratory, Inc.

2.2. Electrode preparation

A commercial FTO glass sheet was cut into small pieces with 1.5 cm × 1.5 cm. The FTO substrates were cleaned in 2-propanol, acetone, and then Milli-Q water under ultrasonication for 20 min each, kept in the mixture of 30% H_2O_2–28% NH_3–Milli-Q water (1:1:5, v/v/v) at 343 K for 1 h, rinsed with Milli-Q water, and then dried under N_2. Pt/FTO and Pd/FTO electrodes were prepared by the deposition of Pt and Pd NPs, respectively, on the FTO substrates at room temperature in the vacuum deposition chamber (Ulvac, MUE-ECO-EV) with ca. 10^{-3} Pa by using coaxial pulsed APD systems (ADVANCE RIKO, ARL-300) [38], in which cylindrical Pt and Pd cathodes were used as sources for Pt and Pd NPs, respectively. The APD of Pt and/or Pd was performed at an arc voltage of 100 V and a condenser capacity of 1080 μF. The APD pulses ranging from 10 to 300 pulses were set to control the amount of Pt and Pd NPs deposited on the FTO substrates, which were placed ca. 7 cm away from the Pt and Pd cathodes. To prepare Pt/Pd/FTO electrodes, Pt and Pd were sequentially deposited on FTO substrates with 30 pulses changing Pt-to-Pd pulse ratio (Pt_x/Pd_{30-x}/FTO, where x (pulse number) = 5, 10, 15, 20, 25). Because almost no effect of the sequential APD order on the NO_3RR activity and particle size was confirmed by electrochemical measurements and TEM images, the experimental data of Pt_x/Pd_{30-x}/FTO are shown and discussed in this work.

2.3. Electrochemical measurements

All cyclic voltammograms (CVs) were recorded using a conventional three-electrode, one compartment electrochemical cell by a potentiostat HZ-5000 (Hokuto Denko Corp.). Pt and/or Pd NPs on FTO substrates were used as working electrodes, and a platinized Pt foil and an Ag|AgCl (sat. KCl) were used as the counter and the reference electrodes, respectively. The geometrical surface area of the working electrode was 0.95 cm^2. Before using, all glassware was immersed in the mixture of 1:1 concentrated nitric and sulfuric acid overnight, rinsed by and boiled in Milli-Q water, and then ultrasonicated. Before measurements of CVs, the electrolyte solution was purged with Ar (99.999%, Hokkaido Air Water Inc.) for at least 30 min. Pt/FTO electrodes were electrochemically

cleaned in the potential range between –0.2 and +1.1 V vs. Ag|AgCl (sat. KCl) at a sweep rate of 0.05 V s^{-1} until getting stable CVs in 0.1 M $HClO_4$ aqueous solution, and the Faradaic charges of hydrogen desorption were used to determine the electrochemically active surface area of Pt ($ECSA_{Pt}$) on FTO substrates. Pd/FTO electrodes were also electrochemically cleaned in 0.1 M $HClO_4$ aqueous solution between +0.1 and +1.1 V vs. Ag|AgCl (sat. KCl) at a sweep rate of 0.05 V s^{-1} until getting stable CVs and the Faradaic charge of PdO_x reduction were used to determine the electrochemically active surface area of Pd ($ECSA_{Pd}$) on FTO substrates. For electrochemical NO_3^- reduction, CVs were recorded in 0.1 M $HClO_4$ aqueous solution containing 0.01 M $NaNO_3$ at a sweep rate of 0.01 V s^{-1}. In the case of electrochemical NO_2^- reduction, 0.0345 g of $NaNO_2$ was added to deaerated 0.1 M $HClO_4$ aqueous solution (50 mL) to make 0.01 M $NaNO_2$ solution just before recording CVs. To investigate the NO electrochemical reduction, a 0.1 M $HClO_4$ aqueous solution was saturated with bubbling of NO gas for 30 min. In this case, NO gas was passed through a 1.0 M NaOH aqueous solution, which removes NO_x, followed by Milli-Q water before being introduced to the electrochemical cell. For electrochemical N_2O reduction, a 0.1 M $HClO_4$ aqueous solution in the electrochemical cell was saturated with bubbling of N_2O gas for 30 min. The first cycle of the CVs was always used for making a graph in presence of the analyte. All potentials shown were converted to be versus the reversible hydrogen electrode (RHE) by using the following equation: E (vs. RHE) = E (vs. Ag|AgCl (sat. KCl)) + 0.199 + 0.059 × pH.

2.4. Physicochemical characterizations

X-ray photoelectron spectroscopy (XPS) data were collected at the pass energy of 10 eV using an Al Kα X-ray source by a photoelectron spectrometer JPS-9200 (JEOL). The C=C peak in the C 1s region was used as an internal standard (284.7 eV) to calibrate the binding energies of the elements. Carbon tape was used to make FTO substrates conductive with the sample holder of XPS, which gave a peak in the C 1s region. Transmission electron microscopy (TEM) images were obtained by JEM-2000FX (JEOL) at an acceleration voltage of 200 kV. Scanning transmission electron microscopy (STEM) and energy dispersive spectroscopy (EDS) elemental mapping images were obtained by JEM-ARM200F (JEOL) at 200 kV. For TEM, STEM, and EDS observations,

Pt and/or Pd NPs were deposited on silicon oxide grids (ALLIANCE Biosystems) to ensure a similar oxide surface to the FTO substrate.

3. Results and discussion

3.1 Characterization of Pt/FTO and Pd/FTO electrodes

To characterize Pt on FTO electrodes with a different number of APD pulses (Pt_x/FTO, where x indicates the number of APD pulses), CVs of Pt_x/FTO were recorded at a sweep rate of 0.05 V s^{-1} in a 0.1 M $HClO_4$ aqueous solution under Ar (Figs. 1a and S1a). Hydrogen adsorption/desorption currents were observed in the potential range between +0.06 and +0.34 V vs. RHE. PtO_x reduction peaks were observed in the potential range between +0.72 and +0.76 V vs. RHE [39]. No such peaks were observed on bare FTO electrodes (gray broken line in Fig. 1a), suggesting the deposition of Pt on FTO. The deposition of Pt NPs was confirmed by TEM observation of model samples of APD–Pt NPs with 30 pulses on a silicon oxide grid (Fig. 1b). A surface density and an averaged diameter of APD–Pt NPs were determined to be 7.1×10^{12} cm^{-2} and 2.2 nm, respectively (Fig. 1c), which is quite close to that previously reported for APD–Pt NPs [28]. For the APD–Pt NPs with 100 pulses, a surface density and an averaged diameter of them were determined to be 9.3×10^{12} cm^{-2} and 2.5 nm, respectively (Fig. S2a and S2b). These results reveal that the surface density of Pt NPs increases with keeping the almost same particle diameter as the number of APD pulses increases. Similar results were reported in a previous study [28]. The APD–Pt NPs with 200 pulses or more gave almost no individual NP, indicating the agglomeration of Pt NPs (Fig. S2c).

The electrochemically active surface area of Pt ($ECSA_{Pt}$) of Pt_x/FTO was calculated using the following equation: $ECSA_{Pt} = Q_H/210$ μC cm^{-2}, where Q_H indicates the Faradaic charges for the hydrogen desorption at the Pt_x/FTO electrodes and 210 μC cm^{-2} corresponds to the Faradaic charge density for the monolayer of the underpotentially deposited hydrogen on the smooth Pt surface [39]. The $ECSA_{Pt}$ was plotted against the number of APD pulses (Fig. S3a). The $ECSA_{Pt}$ of Pt_x/FTO electrodes increases as the number of Pt pulses increases. The $ECSA_{Pt}$ was found to reach a plateau at around 200 Pt pulses due to the formation of a fully covered Pt film on the FTO substrates. A similar plateau region was observed in a previous study on APD–Pt/GC (GC = glassy carbon)

electrodes [28]. Based on the $ECSA_{Pt}$ in the plateau region ($ECSA_{Pt,\ max}$), Pt coverages (θ_{Pt}) on FTO can be defined by the following equation: $\theta_{Pt} = ECSA_{Pt}/ECSA_{Pt,\ max}$.

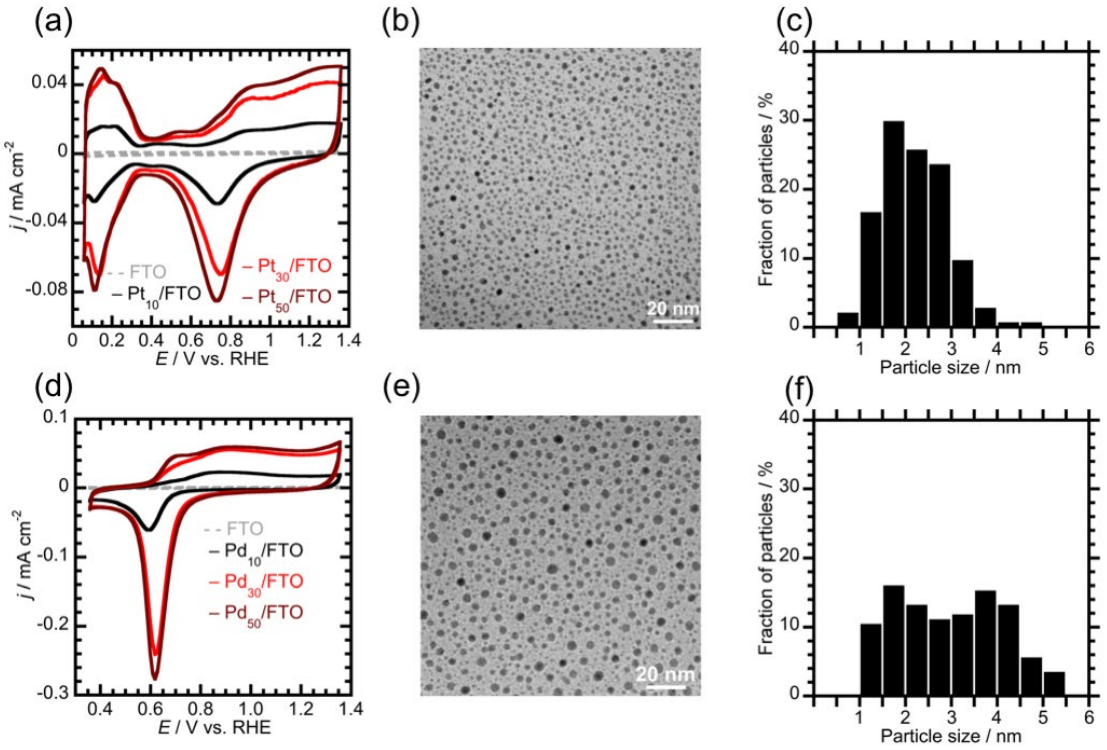


Fig. 1 (a) CVs of Pt_x/FTO electrodes in a 0.1 M $HClO_4$ aqueous solution at a sweep rate of 0.05 V s^{-1} under Ar. (b) TEM image of APD–Pt NPs with 30 pulses on a silicon oxide grid and (c) the histogram of the size distribution of Pt NPs. (d) CVs of Pd_x/FTO electrodes in a 0.1 M $HClO_4$ aqueous solution at a sweep rate of 0.05 V s^{-1} under Ar. (e) TEM image of APD–Pd NPs with 30 pulses on a silicon oxide grid and (f) the histogram of the size distribution of Pd NPs.

CVs of FTO electrodes modified with Pd with a different number of APD pulses (Pd_x/FTO, where x indicates the number of APD pulses) were recorded at 0.05 V s^{-1} in the potential range between +0.36 and +1.36 V vs. RHE in 0.1 M $HClO_4$ aqueous solution under Ar (Figs. 1d and S1b). A reduction peak was observed in the potential range between +0.59 and +0.67 V vs. RHE, which can be associated with the reduction of PdO_x [40,41]. No such peak was observed at the bare FTO electrode (gray dashed line in Fig. 1d). Thus, the deposition of APD–Pd was confirmed on FTO. TEM observation enabled us to determine a Pd NP density and an average diameter to be 3.5×10^{12} cm^{-2} and 3.0

nm for 30 pulses (Figs 1e and 1f) and 3.4×10^{12} cm^{-2} and 3.5 nm for 100 pulses (Fig. S2d and S2e), respectively. Note that increasing the pulse number up to 100 causes almost no change of the Pd NP density but an increase in Pd NP diameter. This trend is different from that of APD-Pt NPs, as mentioned above. The particle size distribution of APD-Pd NPs (Fig. 1f) is wider than that of APD-Pt NPs (Fig. 1c). These results imply that Pd NPs tend to agglomerate on the substrate and/or deposit on Pd NPs already placed on the substrate, whereas Pt NPs tend to individually deposit on the substrate and be less sensitive to agglomeration.

ECSAs of Pd ($ECSA_{Pd}$) on Pd_x/FTO electrodes were determined based on the Faradaic charges for the reduction wave of the surface oxide film in the following equation: $ECSA_{Pd} = Q_{oxide}/424\ \mu C\ cm^{-2}$, where Q_{oxide} indicates the Faradaic charges for the oxide reduction at Pd_x/FTO electrodes and 424 μC cm^{-2} corresponds to the assumed Faradaic charge density for the reduction of surface PdO monolayer on a smooth Pd surface [40]. The $ECSA_{Pd}$ is determined based on the Faradaic charge for the reduction of the surface oxide film, not for the hydrogen adsorption or desorption, because both hydrogen adsorption and absorption occur at the Pd electrode in the same potential range from +0.025 to +0.375 V vs. RHE and they are difficult to be separated [40–43]. The $ECSA_{Pd}$ was plotted against the number of APD pulses (Fig. S3b). The plateau region seems to start at around 300 Pd pulses. Thus, Pd coverages (θ_{Pd}) on the FTO substrates were determined based on the $ECSA_{Pd}$ in the plateau region ($ECSA_{Pd,\ max}$).

3.2 Optimizing NO_3RR at Pt/FTO and Pd/FTO electrodes

CVs of Pt_x/FTO electrodes were recorded in 0.1 M $HClO_4$ aqueous solution containing 0.01 M $NaNO_3$ under Ar (Fig. 2a). All Pt_x/FTO electrodes showed cathodic currents in the potential range from +0.06 to +0.34 V vs. RHE only in the solution containing NO_3^-. These currents can be associated with the electrochemical NO_3RR [20,22,28,30,37]. The NO_3RR current densities of Pt_x/FTO electrodes at +0.16 V vs. RHE were plotted against θ_{Pt} in Fig. 2c [44]. The cathodic current density for the NO_3RR reached the maximum at $\theta_{Pt} \approx 0.63$ (corresponding to Pt_{30}/FTO), which is in good agreement with a previous study [28]. Sn-modified Pt electrodes previously showed the maximum current density for the NO_3RR at a tin coverage of $\theta_{Sn} \approx 0.35$ (–3.6 mA cm^{-2}

at +0.16 V vs. RHE) [22], which is almost the same as $\theta_{Sn} \approx 0.37$ (the residual of $\theta_{Pt} \approx 0.63$) for the Pt_{30}/FTO electrode in this work. Thus, the Pt/Sn interface acts as the active site not only for the electrocatalytic NO_3RR in Sn-modified Pt electrodes but also in the reverse system of Pt_x/FTO [23,44]. The formation of the Pt/Sn interface modifies the electronic state of Pt, supported by XPS (Fig. S4). Pt 4f peaks at Pt_{30}/FTO shifted to the lower binding energy than those at Pt_{30}/GC (Fig. S4b and Table S1). These results suggest the charge transfer from Sn in FTO to Pt. Note that no clear binding energy shift was observed in the Sn 3d region (Table S2) because many Sn species of FTO show no direct interaction with Pt NPs, whereas most of Pt NPs interact with Sn species of FTO.

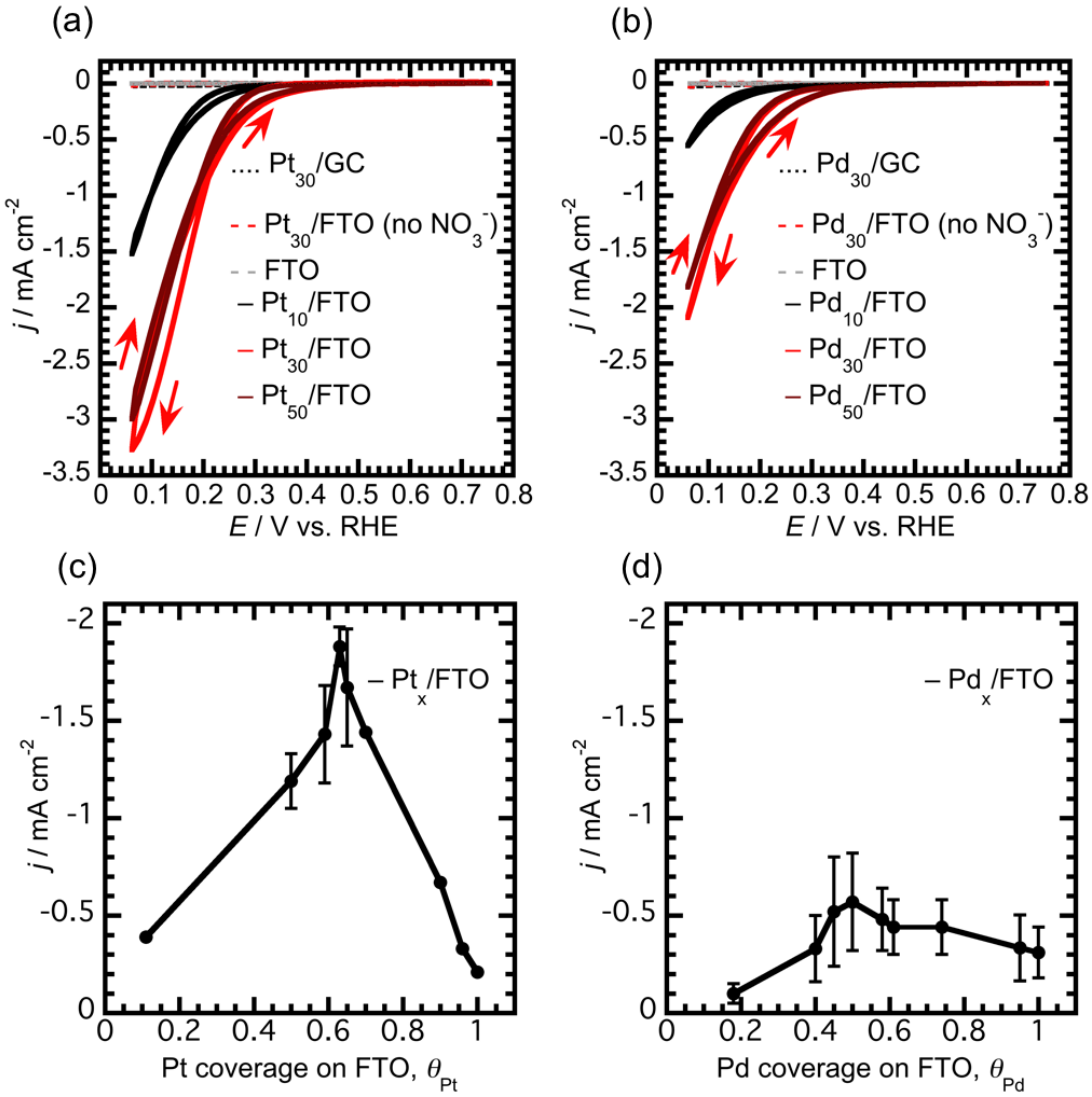


Fig. 2 CVs of (a) Pt_x/FTO and (b) Pd_x/FTO electrodes in a 0.1 M $HClO_4$ aqueous solution containing 0.01 M $NaNO_3$ at 0.01 V s^{-1} under Ar. The plots of (c) Pt and (d) Pd coverage-dependent current density for the NO_3RR at +0.16 V vs. RHE.

Pd_x/FTO electrodes also showed the NO_3RR activity (Fig. 2b). The cathodic current densities for the NO_3RR at +0.16 V vs. RHE were plotted against θ_{Pd} (Fig. 2d). The reduction current density increased with increasing θ_{Pd} up to $\theta_{Pd} \approx 0.50$ (corresponding to Pd_{30}/FTO) and then remained almost constant. Since no plateau region is observed for Pt_x/FTO (Fig. 2c), the θ_{Pd} dependence of Pd_x/FTO on the NO_3RR activity is different from the θ_{Pt} dependence of Pt_x/FTO. This difference could be related to the difference in the APD process between Pt and Pd as mentioned above: the agglomeration tendency of Pd NPs but not in the case of Pt NPs during ADP process (See Section 3.1). The Pd_{30}/FTO electrode with $\theta_{Pd} \approx 0.50$ showed the highest electrocatalytic NO_3RR current density of ca. –0.57 mA cm^{-2} at +0.16 V vs. RHE in the Pd_x/FTO electrodes (Table S3) and the charge transfer from Sn to Pd was confirmed by the comparison of XPS data of Pd_{30}/FTO with Pd_{30}/GC in the Pd 3d region (Fig. S4 and Tables S1).

The Pt_{30}/FTO electrode with $\theta_{Pt} \approx 0.63$ showed greater activity for the NO_3RR than the Pd_{30}/FTO electrode with $\theta_{Pd} \approx 0.50$ (Fig. 2 and Table S3), indicating that the Pt/Sn interface more efficiently catalyzes the NO_3RR than the Pd/Sn interface. A similar activity trend for the NO_3RR was reported in a previous study on Sn-modified noble metals: Sn-modified Pt electrodes showed higher NO_3RR activity than Sn-modified Pd electrodes [13]. Although the charge densities of Pt and Pd are modulated by charge transfer from Sn, the activity difference between Pt_{30}/FTO and Pd_{30}/FTO can be explained by the intrinsic difference between NO_3^- adsorption energies on Pt and Pd: NO_3^- adsorption energy on Pt surface (–2.23 eV) was reported to be higher than that on Pd surface (–2.14 eV) [45].

3.3. NO_3RR at Pt/Pd/FTO electrodes

For a ternary metallic system, Pt and Pd NPs were deposited on FTO substrates by the APD with 30 pulses changing Pt–to–Pd–pulses ratios (Pt_x/Pd_{30-x}/FTO, where x (pulse number) = 5, 10, 15, 20, 25). The total pulse number is based on the optimized pulse number for the bimetallic systems of Pt_{30}/FTO and Pd_{30}/FTO. The Pt_{15}/Pd_{15}/FTO electrode showed the highest NO_3RR activity of –2.24 mA cm^{-2} at +0.16 V vs. RHE in

the Pt_x/Pd_{30-x}/FTO electrodes (Figs. 3, S5, and Table S4). In the following text, the optimized ternary and binary metallic electrodes of Pt_{15}/Pd_{15}/FTO, Pt_{30}/FTO, and Pd_{30}/FTO prepared by the APD method are referred as to Pt/Pd/FTO, Pt/FTO, and Pd/FTO, respectively.

The optimized ternary metallic electrode shows higher NO_3RR activity than the binary metallic electrodes: the order of NO_3RR activity was found as follows: Pt/Pd/FTO > Pt/FTO > Pd/FTO (Fig. 3a). Similar results have also been reported for Sn-modified PdPt electrodes [13,30]. TEM, STEM, and EDS mapping images of Pt/Pd (Pt_{15}/Pd_{15}) on silicon oxide grids confirmed a particle density of 7.5×10^{12} cm^{-2} with an average diameter of 2.3 nm and the co-presence of Pt and Pd as a mixture in NPs with an atomic ratio to 3:2 (Fig. 4). Furthermore, a Pt/Pd/GC electrode as a control sample showed almost no activity for the NO_3RR (Fig. 3b). Thus, the ternary metallic PtPd/Sn interface of Pt/Pd/FTO plays an important role in the high NO_3RR activity.

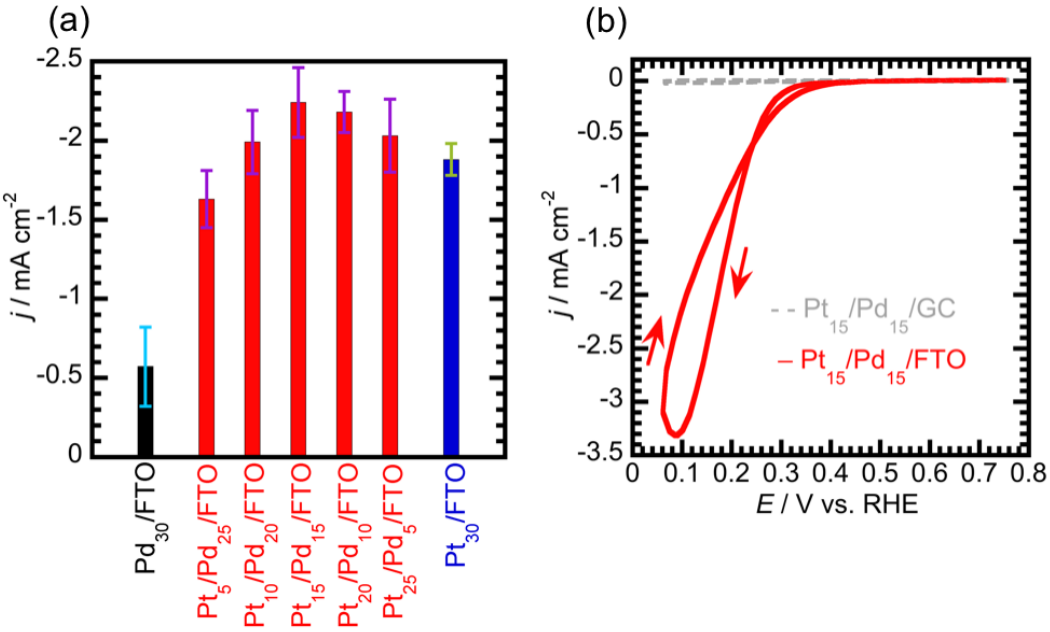


Fig. 3 (a) Bar graph of current densities for the NO_3RR at +0.16 V vs. RHE shown by Pt_{30}/FTO, Pd_{30}/FTO, and Pt_x/Pd_{30-x}/FTO electrodes. (b) CVs of Pt_{15}/Pd_{15}/GC and Pt_{15}/Pd_{15}/FTO electrodes in 0.1 M $HClO_4$ aqueous solution containing 0.01 M $NaNO_3$ at a sweep rate of 0.01 V s^{-1} under Ar.

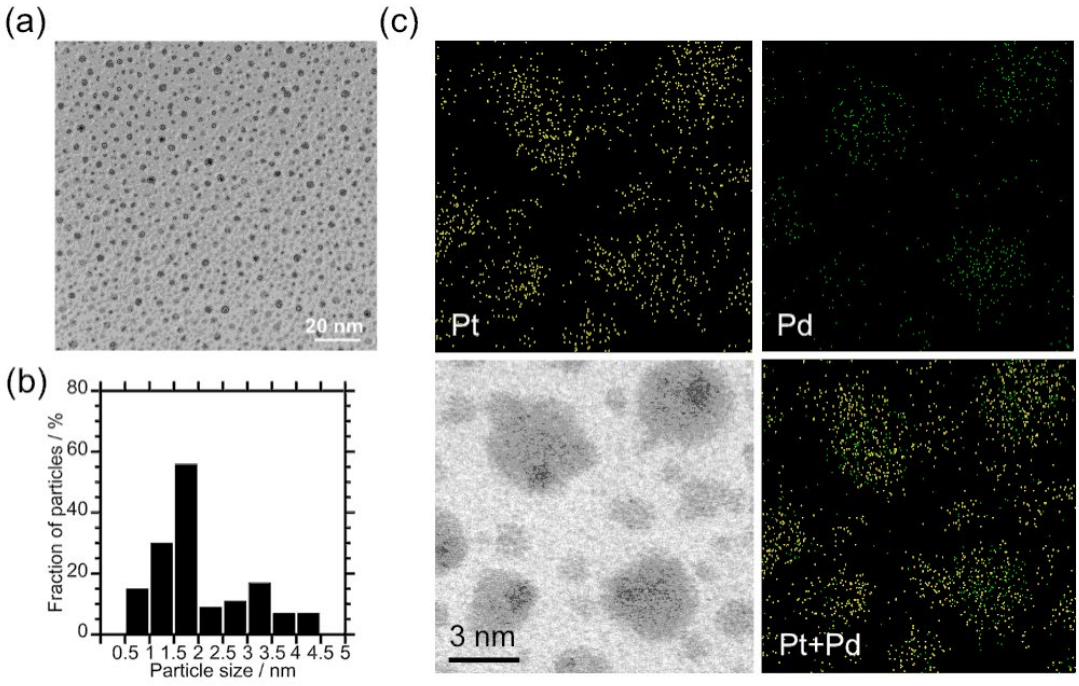


Fig. 4 (a) TEM image, (b) size distribution, and (c) STEM image and EDS mapping of Pt/Pd NPs (Pt_{15}/Pd_{15}) on a silicon oxide grid. The yellow and green color images indicate the Pt and Pd elements, respectively.

The Pt/Pd/FTO electrode showed cathodic currents for the NO_3RR in the potential region between +0.06 and +0.34 V vs. RHE (Fig. 3b). In this potential region, the adsorption of NO_3^- competes with the hydrogen adsorption (Fig. S6) [14,35,45]. The formation of the PtPd/Sn interface could enhance the NO_3^- adsorption and/or suppress the hydrogen adsorption [30], and then accelerate the rate-determining step of the NO_3^- reduction to NO_2^- [11,24,29]. This explanation can be supported by the observation of the charge transfer from Sn to Pt and Pd for the Pt/Pd/FTO like the binary metallic systems: lower binding energy shifts than Pt/Pd/GC in the Pt 4f and Pd 3d regions (Fig. 5 and Tables S5 and S6). Thus, the ternary metallic PtPd/Sn interface enables us to finely tune the adsorption ability of NO_3^-, resulting in the high NO_3RR activity.

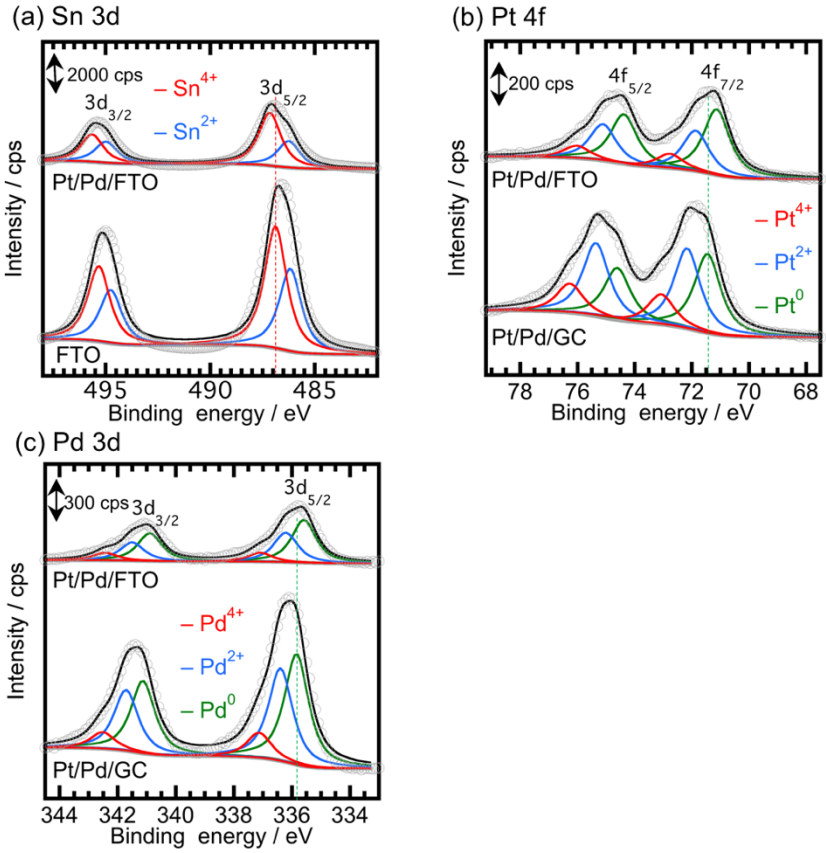


Fig. 5 XPS of (a) Pt/Pd/FTO and FTO electrodes in the Sn 3d region, Pt/Pd/FTO and Pt/Pd/GC electrodes in the (b) Pt 4f, and (c) Pd 3d regions. Experimental data (open circles), the sum of the deconvoluted data (solid line in black), and baseline (in gray).

3.4. NO_2RR, NORR, and N_2ORR at Pt/Pd/FTO and Pt/Pd/GC electrodes

The high NO_3RR activity of the ternary metallic Pt/Pd/FTO encourages us to study NO_2RR, NORR, and N_2ORR using Pt/Pd/FTO and Pt/Pd/GC electrodes to further understand the role of the PtPd/Sn interface into the production of N_2 in the electrocatalytic NO_3RR. Pt/Pd/FTO showed much higher cathodic currents than Pt/Pd/GC in a 0.1 M $HClO_4$ aqueous solution under N_2O (Fig. 6a). Although Pd/FTO and Pt/FTO also showed the electrocatalytic N_2ORR activity (Fig. S7), the activity of Pt/Pd/FTO was higher than those of Pd/FTO and Pt/FTO (Table S7). Therefore, the formation of the PtPd/Sn interface increases not only the NO_3RR activity but also the N_2ORR activity. The cathodic currents of Pt/Pd/FTO for the N_2ORR can be mainly found in the hydrogen adsorption region between +0.06 and +0.34 V vs. RHE (Fig. S6). The

N_2O adsorption can compete with the hydrogen adsorption on Pt and Pd electrodes [46–48]. The PtPd/Sn interface could enhance the N_2O adsorption and/or suppress the hydrogen adsorption, leading to the enhancement of the N_2ORR activity.

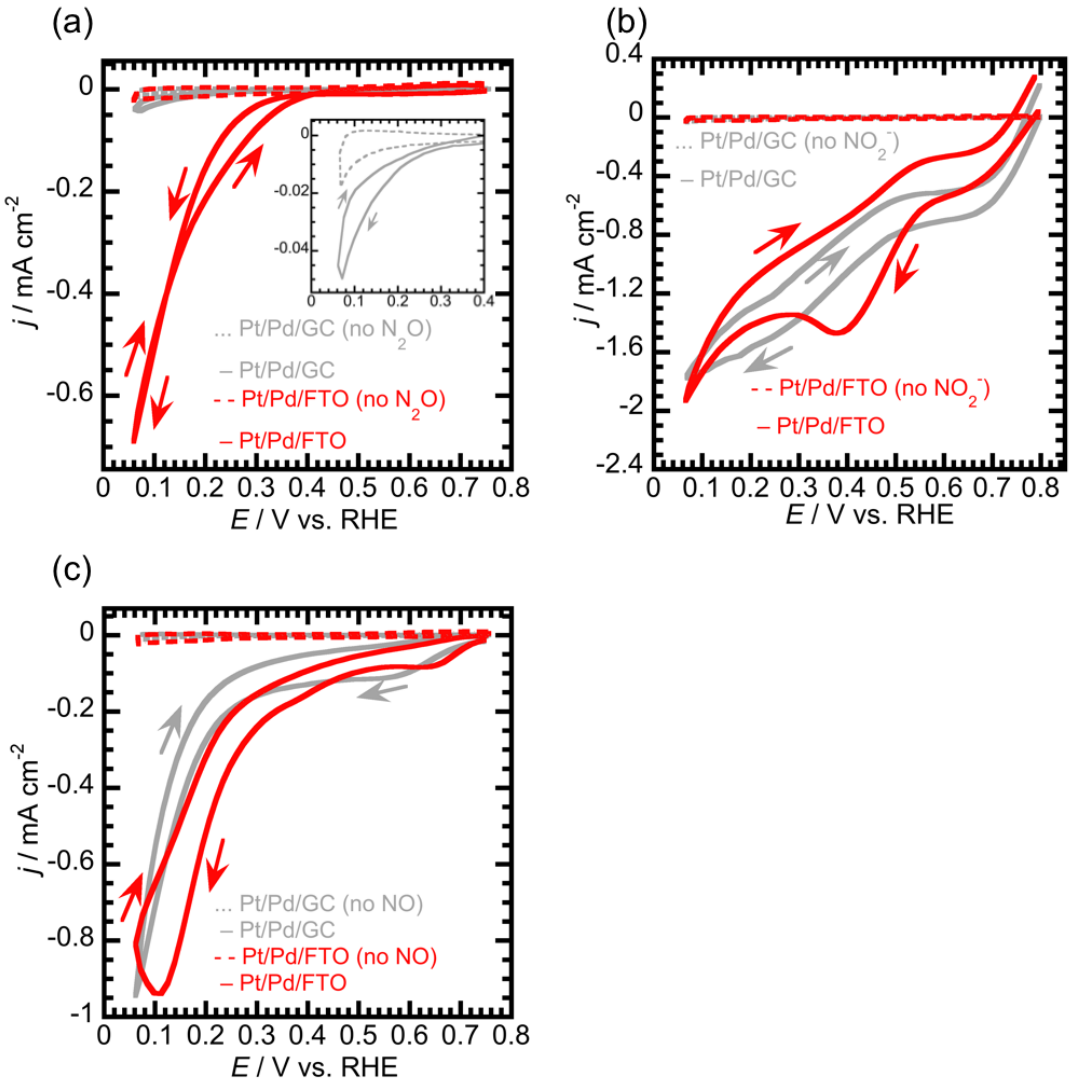
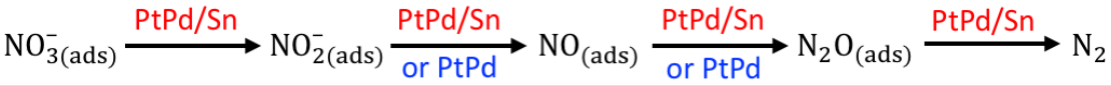


Fig. 6 CVs of Pt/Pd/GC and Pt/Pd/FTO electrodes at a sweep rate of 0.01 V s^{-1} in an aqueous solution of 0.1 M $HClO_4$ (a) under N_2O (The inset shows the magnified CVs of Pt/Pd/GC electrode), (b) containing 0.01 M $NaNO_2$ under Ar, and (c) under NO.

Pt/Pd/FTO and Pt/Pd/GC electrodes show similar cathodic currents for the NO_2RR and NORR, as shown in Fig. 6b and 6c, respectively, indicating almost no difference in the NO_2RR and NORR activity between Pt/Pd/FTO and Pt/Pd/GC. This finding indicates that Sn shows no drastic contribution to the activity improvement for

the NO_2RR and NORR. Because the NO_2RR and NORR mainly occur at more positive potentials than the hydrogen adsorption, NO_2^- or NO adsorption does not compete with the hydrogen adsorption, resulting in no contribution of the ternary interface including Sn to the activity enhancement.



Scheme 1: Highly active catalytic sites for the electrocatalytic NO_3RR, NO_2RR, NORR, and N_2ORR.

For the Pt/Pd/FTO electrode, the PtPd/Sn interface efficiently catalyzed the NO_3RR and N_2ORR but not the NO_2RR and NORR **(Scheme 1)**. The NO_3RR and N_2ORR occur in the potential range of the hydrogen adsorption between +0.06 and +0.34 V vs. RHE (Fig. S6). Since the adsorption of NO_3^- or N_2O competes with hydrogen adsorption on Pt and Pd electrodes in this potential region, the PtPd/Sn interface enhanced the adsorption of NO_3^- or N_2O and/or suppressed the adsorption of hydrogen. As a consequence, the activity of NO_3RR and N_2ORR increased and less hydrogen at the PtPd/Sn interface may favor the formation of the most likely product N_2 instead of the formation of NH_4^+ and NH_3OH^+ [12–14,49]. In contrast, because of no overlap of onset potentials of the NO_2RR and NORR with hydrogen adsorption, Sn did not work as a promoter for the NO_2RR and NORR.

4. Conclusions

Our study demonstrates that the PtPd/Sn interface is effective to the electrocatalytic NO_3RR and N_2ORR, whereas it showed no drastic contribution to the electrocatalytic NO_2RR and NORR. It is most likely that the ternary metallic PtPd/Sn interface enhances the adsorption of NO_3^- and N_2O and/or suppressed the adsorption of hydrogen. XPS data of the Pt/Pd/FTO electrode revealed the charge transfer from Sn in FTO to Pt and Pd, suggesting the modulation of the adsorption ability of NO_3^-, N_2O, and hydrogen at the PtPd/Sn interface. Our findings will be helpful to develop highly efficient noble metal mixture/alloy NPs on FTO support electrodes for the practical application of denitrification.

Acknowledgments

The authors thank Shingo Mukai and Yusuke Kawamura (Technical Division, Institute for Catalysis, Hokkaido University) for their technical support on the modification of our APD setup; Takashi Tanioka and Ryoko Yokohira (Faculty of Engineering, Hokkaido University) for taking TEM images; Naomi Hirai and Yuko Mori (Research Institute for Electronic Science, Hokkaido University) for taking the STEM and EDS mapping images, and XPS data. This work was financially supported by the Ministry of Education, Culture, Sports, Science and Technology (MEXT), Japan, JSPS KAKENHI Grant numbers JP16K20882, JP21K05124 (to MK), and JP19H02664 (to IY), and the "Nanotechnology Platform" program of the MEXT for Hokkaido University (JPMXP09A18HK0063, 19HK0030 and 21HK0062).

References

[1] A. Scheidleder, J. Grath, G. Winkler, U. Stärk, C. Koreimann, C. Gmeiner, S. Nixon, J. Casillas, P. Gravesen, J. Leonard, M. Elvira, Groundwater quality and quantity in Europe, Eur. Environ. Agency. (1999) 1–123. https://www.eea.europa.eu/publications/TEC22.

[2] C.J. Johnson, B.C. Kross, Continuing importance of nitrate contamination of groundwater and wells in rural areas, Am. J. Ind. Med. 18 (1990) 449–456. https://doi.org/10.1002/ajim.4700180416.

[3] R.R. Jones, P.J. Weyer, C.T. Dellavalle, M. Inoue-Choi, K.E. Anderson, K.P. Cantor, S. Krasner, K. Robien, L.E. Beane Freeman, D.T. Silverman, M.H. Ward, Nitrate from drinking water and diet and bladder cancer among postmenopausal women in Iowa, Environ. Health Perspect. 124 (2016) 1751–1758. https://doi.org/10.1289/EHP191.

[4] H. Tian, R. Xu, J.G. Canadell, R.L. Thompson, W. Winiwarter, P. Suntharalingam, E.A. Davidson, P. Ciais, R.B. Jackson, G. Janssens-Maenhout, M.J. Prather, P. Regnier, N. Pan, S. Pan, G.P. Peters, H. Shi, F.N. Tubiello, S. Zaehle, F. Zhou, A. Arneth, G. Battaglia, S. Berthet, L. Bopp, A.F. Bouwman, E.T. Buitenhuis, J. Chang, M.P. Chipperfield, S.R.S. Dangal, E. Dlugokencky, J.W. Elkins, B.D. Eyre, B. Fu, B. Hall, A. Ito, F. Joos, P.B. Krummel, A. Landolfi, G.G. Laruelle, R. Lauerwald, W. Li, S. Lienert, T. Maavara, M. MacLeod, D.B. Millet, S. Olin, P.K. Patra, R.G. Prinn, P.A. Raymond, D.J. Ruiz, G.R. van der Werf, N. Vuichard, J. Wang, R.F. Weiss, K.C. Wells, C. Wilson, J. Yang, Y. Yao, A comprehensive quantification of global nitrous oxide sources and sinks, Nature. 586 (2020) 248–256. https://doi.org/10.1038/s41586-020-2780-0.

[5] K. Parris, Impact of agriculture on water pollution in OECD countries: Recent trends and future prospects, Int. J. Water Resour. Dev. 27 (2011) 33–52. https://doi.org/10.1080/07900627.2010.531898.

[6] Y.Y. Yang, G.S. Toor, Sources and mechanisms of nitrate and orthophosphate transport in urban stormwater runoff from residential catchments, Water Res. 112 (2017) 176–184. https://doi.org/10.1016/j.watres.2017.01.039.

[7] M.H. Ward, R.R. Jones, J.D. Brender, T.M. de Kok, P.J. Weyer, B.T. Nolan, C.M. Villanueva, S.G. van Breda, Drinking water nitrate and human health: An updated review, Int. J. Environ. Res. Public Health. 15 (2018) 1–31. https://doi.org/10.3390/ijerph15071557.

[8] Guidelines for Drinking-water Quality, World Health Organization, 4th ed., 2011. https://doi.org/10.1007/978-1-4020-4410-6_184.

[9] M. Duca, M.T.M. Koper, Powering denitrification: The perspectives of electrocatalytic nitrate reduction, Energy Environ. Sci. 5 (2012) 9726–9742. https://doi.org/10.1039/c2ee23062c.

[10] N. Singh, B.R. Goldsmith, Role of Electrocatalysis in the Remediation of Water Pollutants, ACS Catal. 10 (2020) 3365–3371. https://doi.org/10.1021/acscatal.9b04167.

[11] M. Kato, Y. Unuma, M. Okui, Y. Qu, J. Zheng, S. Taguchi, F. Kiguchi, M. Torihata, Y. Gao, N. Hoshi, I. Yagi, Electrocatalytic activity and volatile product selectivity for nitrate reduction at tin-modified Pt(100), Pd(100) and Pd–Pt(100) single crystal electrodes in acidic media, Electrochim. Acta. 398 (2021) 139281.

https://doi.org/10.1016/j.electacta.2021.139281.
[12] J. Souza-Garcia, E.A. Ticianelli, V. Climent, J.M. Feliu, Mechanistic changes observed in heavy water for nitrate reduction reaction on palladium-modified Pt(hkl) electrodes, Chem. Sci. 3 (2012) 3063–3070. https://doi.org/10.1039/c2sc20490h.
[13] M.M. Hossain, T. Kawaguchi, K. Shimazu, K. Nakata, Reduction of nitrate on tin-modified palladium-platinum electrodes, J. Electroanal. Chem. 864 (2020). https://doi.org/10.1016/j.jelechem.2020.114041.
[14] G.E. Dima, A.C.A. De Vooys, M.T.M. Koper, Electrocatalytic reduction of nitrate at low concentration on coinage and transition-metal electrodes in acid solutions, J. Electroanal. Chem. 554–555 (2003) 15–23. https://doi.org/10.1016/S0022-0728(02)01443-2.
[15] Y.Y. Birdja, J. Yang, M.T.M. Koper, Electrocatalytic reduction of nitrate on tin-modified palladium electrodes, Electrochim. Acta. 140 (2014) 518–524. https://doi.org/10.1016/j.electacta.2014.06.011.
[16] van V.J.A.R. de Vooys, A. C.A., van Santen, R.A., Electrocatalytic reduction of NO3- on palladium/copper electrodes, J. Mol. Catal. A Chem. 154 (2000) 203–215. https://doi.org/10.1007/978-3-319-61112-9_2.
[17] V. Rosca, M. Duca, M.T. DeGroot, M.T.M. Koper, Nitrogen Cycle Electrocatalysis, Chem. Rev. 109 (2009) 2209–2244. https://doi.org/10.1021/cr8003696.
[18] S. Taguchi, J.M. Feliu, Electrochemical reduction of nitrate on Pt(S)[n(1 1 1) × (1 1 1)] electrodes in perchloric acid solution, Electrochim. Acta. 52 (2007) 6023–6033. https://doi.org/10.1016/j.electacta.2007.03.057.
[19] M.C. Figueiredo, J. Solla-Gullón, F.J. Vidal-Iglesias, V. Climent, J.M. Feliu, Nitrate reduction at Pt(1 0 0) single crystals and preferentially oriented nanoparticles in neutral media, Catal. Today. 202 (2013) 2–11. https://doi.org/10.1016/j.cattod.2012.02.038.
[20] J. Yang, F. Calle-Vallejo, M. Duca, M.T.M. Koper, Electrocatalytic reduction of nitrate on a Pt electrode modified by p-block metal adatoms in acid solution, ChemCatChem. 5 (2013) 1773–1783. https://doi.org/10.1002/cctc.201300075.
[21] K. Shimazu, R. Goto, S. Piao, R. Kayama, K. Nakata, Y. Yoshinaga, Reduction of nitrate ions on tin-modified palladium thin film electrodes, J. Electroanal. Chem. 601 (2007) 161–168. https://doi.org/10.1016/j.jelechem.2006.11.005.
[22] K. Shimazu, R. Goto, K. Tada, Electrochemical reduction of nitrate ions on tin-modified platinum and palladium electrodes, Chem. Lett. 31 (2002) 204–205. https://doi.org/10.1246/cl.2002.204.
[23] J. Yang, M. Duca, K.J.P. Schouten, M.T.M. Koper, Formation of volatile products during nitrate reduction on a Sn-modified Pt electrode in acid solution, J. Electroanal. Chem. 662 (2011) 87–92. https://doi.org/10.1016/j.jelechem.2011.03.015.
[24] J. Yang, Y. Kwon, M. Duca, M.T.M. Koper, Combining voltammetry and ion chromatography: Application to the selective reduction of nitrate on Pt and PtSn electrodes, Anal. Chem. 85 (2013) 7645–7649. https://doi.org/10.1021/ac401571w.
[25] M. Motahar Hossain, K. Nakata, T. Kawaguchi, K. Shimazu, Reduction of nitrate on electrochemically pre-reduced tin-modified palladium electrodes, J.

Electroanal. Chem. 707 (2013) 59–65. https://doi.org/10.1016/j.jelechem.2013.08.015.
[26] O. Ghodbane, M. Sarrazin, L. Roué, D. Bélanger, Electrochemical Reduction of Nitrate on Pyrolytic Graphite-Supported Cu and Pd–Cu Electrocatalysts, J. Electrochem. Soc. 155 (2008) F117. https://doi.org/10.1149/1.2900094.
[27] S. Piao, Y. Kayama, Y. Nakano, K. Nakata, Y. Yoshinaga, K. Shimazu, Nitrate reduction on tin-modified rhodium, ruthenium, and iridium electrodes, J. Electroanal. Chem. 629 (2009) 110–116. https://doi.org/10.1016/j.jelechem.2009.01.031.
[28] M. Kato, A. Araki, Y. Hara, S. Taguchi, I. Yagi, Cathodic arc-plasma deposition of platinum nanoparticles on fluorine-doped tin oxide for electrocatalytic nitrate reduction reaction, Electrochemistry. 86 (2018) 220–222. https://doi.org/10.5796/electrochemistry.18-00031.
[29] J.F.E. Gootzen, P.G.J.M. Peeters, J.M.B. Dukers, L. Lefferts, W. Visscher, J.A.R. Van Veen, The electrocatalytic reduction of NO-3 on Pt, Pd and Pt + Pd electrodes activated with Ge, J. Electroanal. Chem. 434 (1997) 171–183. https://doi.org/10.1016/S0022-0728(97)00093-4.
[30] M. Kato, M. Okui, S. Taguchi, I. Yagi, Electrocatalytic nitrate reduction on well-defined surfaces of tin-modified platinum, palladium and platinum-palladium single crystalline electrodes in acidic and neutral media, J. Electroanal. Chem. 800 (2017) 46–53. https://doi.org/10.1016/j.jelechem.2017.01.020.
[31] T. Yoshioka, K. Iwase, S. Nakanishi, K. Hashimoto, K. Kamiya, Electrocatalytic Reduction of Nitrate to Nitrous Oxide by a Copper-Modified Covalent Triazine Framework, J. Phys. Chem. C. 120 (2016) 15729–15734. https://doi.org/10.1021/acs.jpcc.5b10962.
[32] J. Shen, Y.Y. Birdja, M.T.M. Koper, Electrocatalytic Nitrate Reduction by a Cobalt Protoporphyrin Immobilized on a Pyrolytic Graphite Electrode, Langmuir. 31 (2015) 8495–8501. https://doi.org/10.1021/acs.langmuir.5b00977.
[33] Y. Chen, H. Zhu, M. Rasmussen, D. Scherson, Rational design of electrocatalytic interfaces: The multielectron reduction of nitrate in aqueous electrolytes, J. Phys. Chem. Lett. 1 (2010) 1907–1911. https://doi.org/10.1021/jz1005253.
[34] P. Tavares, A.S. Pereira, J.J.G. Moura, I. Moura, Metalloenzymes of the denitrification pathway, J. Inorg. Biochem. 100 (2006) 2087–2100. https://doi.org/10.1016/j.jinorgbio.2006.09.003.
[35] G.E. Dima, V. Rosca, M.T.M. Koper, Role of germanium in promoting the electrocatalytic reduction of nitrate on platinum: An FTIR and DEMS study, J. Electroanal. Chem. 599 (2007) 167–176. https://doi.org/10.1016/j.jelechem.2005.12.005.
[36] J. Lim, C.Y. Liu, J. Park, Y.H. Liu, T.P. Senftle, S.W. Lee, M.C. Hatzell, Structure Sensitivity of Pd Facets for Enhanced Electrochemical Nitrate Reduction to Ammonia, ACS Catal. 11 (2021) 7568–7577. https://doi.org/10.1021/acscatal.1c01413.
[37] K. Nakata, Y. Doi, S. Kubota, K. Shimazu, Reduction of nitrite on tin-modified noble metal electrodes, J. Electroanal. Chem. 647 (2010) 187–193. https://doi.org/10.1016/j.jelechem.2010.06.003.
[38] S. Hinokuma, S. Misumi, H. Yoshida, M. Machida, Nanoparticle catalyst preparation using pulsed arc plasma deposition, Catal. Sci. Technol. 5 (2015)

4249–4257. https://doi.org/10.1039/c5cy00636h.
[39] M. Lukaszewski, M. Soszko, A. Czerwiński, Electrochemical methods of real surface area determination of noble metal electrodes - an overview, Int. J. Electrochem. Sci. 11 (2016) 4442–4469. https://doi.org/10.20964/2016.06.71.
[40] M. Grdeń, M. Łukaszewski, G. Jerkiewicz, A. Czerwiński, Electrochemical behaviour of palladium electrode: Oxidation, electrodissolution and ionic adsorption, Electrochim. Acta. 53 (2008) 7583–7598. https://doi.org/10.1016/j.electacta.2008.05.046.
[41] L.H. Dall'Antonia, G. Tremiliosi-Filho, G. Jerkiewicz, Influence of temperature on the growth of surface oxides on palladium electrodes, J. Electroanal. Chem. 502 (2001) 72–81. https://doi.org/10.1016/S0022-0728(00)00505-2.
[42] C. Gabrielli, P.P. Grand, A. Lasia, H. Perrot, Investigation of Hydrogen Adsorption and Absorption in Palladium Thin Films, J. Electrochem. Soc. 151 (2004) A1937. https://doi.org/10.1149/1.1797035.
[43] I. Achari, S. Ambrozik, N. Dimitrov, Electrochemical Atomic Layer Deposition of Pd Ultrathin Films by Surface Limited Redox Replacement of Underpotentially Deposited H in a Single Cell, J. Phys. Chem. C. 121 (2017) 4404–4411. https://doi.org/10.1021/acs.jpcc.6b12794.
[44] K. Tada, K. Shimazu, Kinetic studies of reduction of nitrate ions at Sn-modified Pt electrodes using a quartz crystal microbalance, J. Electroanal. Chem. 577 (2005) 303–309. https://doi.org/10.1016/j.jelechem.2004.11.039.
[45] J.X. Liu, D. Richards, N. Singh, B.R. Goldsmith, Activity and Selectivity Trends in Electrocatalytic Nitrate Reduction on Transition Metals, ACS Catal. 9 (2019) 7052–7064. https://doi.org/10.1021/acscatal.9b02179.
[46] H. Ebert, R. Parsons, G. Ritzoulis, T. VanderNoot, The reduction of nitrous oxide on platinum electrodes in acid solution, J. Electroanal. Chem. 264 (1989) 181–193. https://doi.org/10.1016/0022-0728(89)80156-1.
[47] A. Ahmadi, E. Bracey, R. Wyn Evans, G. Attard, Anion-surface interactions. Part II. Nitrous oxide reduction as a probe of anion adsorption on transition metal surfaces, J. Electroanal. Chem. 350 (1993) 297–316. https://doi.org/10.1016/0022-0728(93)80212-Z.
[48] A. Aziznia, A. Bonakdarpour, E.L. Gyenge, C.W. Oloman, Electroreduction of nitrous oxide on platinum and palladium: Toward selective catalysts for methanol-nitrous oxide mixed-reactant fuel cells, Electrochim. Acta. 56 (2011) 5238–5244. https://doi.org/10.1016/j.electacta.2011.03.023.
[49] J. Souza-Garcia, E.A. Ticianelli, V. Climent, J.M. Feliu, Nitrate reduction on Pt single crystals with Pd multilayer, Electrochim. Acta. 54 (2009) 2094–2101. https://doi.org/10.1016/j.electacta.2008.08.059.